

RESEARCH ARTICLE | OCTOBER 02 2025

The effect of stress on thermoelectric properties of flexible Mg_3Bi_2 thin films

Grzegorz Sadowski ; Arnaud le Febvrier ; Johan Hektor ; Per Eklund ; Denis Music 

 Check for updates

Appl. Phys. Lett. 127, 133102 (2025)

<https://doi.org/10.1063/5.0280888>



Articles You May Be Interested In

Epitaxial growth and thermoelectric properties of Mg_3Bi_2 thin films deposited by magnetron sputtering

Appl. Phys. Lett. (February 2022)

Structural evolution and thermoelectric properties of $Mg_3Sb_xBi_{2-x}$ thin films deposited by magnetron sputtering

J. Vac. Sci. Technol. A (June 2023)

The role of spin-orbit interaction in low thermal conductivity of Mg_3Bi_2

Appl. Phys. Lett. (December 2023)

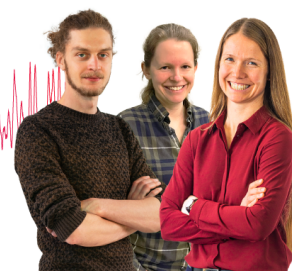
Webinar From Noise to Knowledge

May 13th – Register now



Zurich Instruments

Universität Konstanz



The effect of stress on thermoelectric properties of flexible Mg_3Bi_2 thin films

Cite as: Appl. Phys. Lett. **127**, 133102 (2025); doi: [10.1063/5.0280888](https://doi.org/10.1063/5.0280888)

Submitted: 15 May 2025 · Accepted: 19 September 2025 ·

Published Online: 2 October 2025



View Online



Export Citation



CrossMark

Grzegorz Sadowski,^{1,2,a)}  Arnaud le Febvrier,³  Johan Hektor,^{1,2}  Per Eklund,^{3,4}  and Denis Music^{1,2} 

AFFILIATIONS

¹Department of Materials Science and Applied Mathematics, Malmö University, SE-205 06 Malmö, Sweden

²Biofilms Research Center for Biointerfaces, Malmö University, SE-205 06 Malmö, Sweden

³Department of Chemistry—Ångström Laboratory, Uppsala University, SE-751 21 Uppsala, Sweden

⁴Thin Film Physics Division, Department of Physics, Chemistry and Biology, (IFM), Linköping University, SE-58183 Linköping, Sweden

^{a)} Author to whom correspondence should be addressed: grzegorz.sadowski@mau.se

ABSTRACT

Mechanically flexible thermoelectric materials are of importance for energy harvesting and powering portable and wearable devices. Stress is often disregarded in investigations of thermoelectric properties, despite the fact that it is increasingly important for flexible devices, given the known but often overlooked correlations between stress and physical properties. To investigate the effects of stress on the thermoelectric properties of Mg_3Bi_2 , we synthesized thin films between ambient temperature and 190 °C using magnetron sputtering. Polymeric and ceramic substrates with a wide range of thermal expansion coefficients were used to grow thin films with varied thermal stress. The crystal structure, morphology, and transport properties of the films were explored. The results indicate that low to moderate stress is beneficial for the power factor, ranging from 0.2 to 152 $\mu\text{W m}^{-1} \text{K}^{-2}$ at zero thermal stress and 46 MPa, respectively. This highlights the importance of stating stress with the thermoelectric results and could help explain the extensive scatter of literature values reported for the same thermoelectric systems.

© 2025 Author(s). All article content, except where otherwise noted, is licensed under a Creative Commons Attribution (CC BY) license (<https://creativecommons.org/licenses/by/4.0/>). <https://doi.org/10.1063/5.0280888>

Mechanically flexible thermoelectrics provide a convenient power source for wearable devices.^{1–3} Wearable electronics can be embedded in accessories and clothes, or even directly attached to the skin.⁴ They are essential for personalized healthcare and communication.¹ Currently, wearable devices are mostly powered by batteries, which are required to be small, light, mechanically flexible, and have a long lifetime. The last requirement is not only crucial for medical applications but also necessary to keep the economic and environmental costs low.⁴ However, these requirements pose a major challenge for batteries, since they are required to be periodically recharged, replaced, or otherwise maintained.^{3,5} Thermoelectric thin films can potentially substitute batteries, providing uninterrupted power by converting the heat energy from human skin into electricity. They are reliable and silent since there are no moving parts, and they do not require maintenance. Synthesizing thermoelectric materials in the form of thin films can confer them flexibility and is also convenient for the production of microdevices.⁶ Furthermore, the synthesis process for thin films allows for high control over the residual stress.

Despite studies showing the potential benefits of controlling stress in various materials,^{7–13} it is often ignored or overlooked in conjunction with thermoelectric properties. At the same time, excessive stress in the thin film can cause cracks, buckling, and even delamination.¹⁴ The synthesis of thin films can result in non-equilibrium structures, with atoms displaced from their equilibrium positions inducing intrinsic stress. Additionally, the energetic metal ions present in plasma during physical vapor deposition may further cause stress to build up in the film, as can the lattice mismatch between the film and substrate. The difference in thermal expansion coefficients can induce thermal stress,¹⁵ whereby the residual stress of the film is the sum of all these factors. Controlling stress can help improve desired properties. However, correlations between stress and thermoelectric properties are often unknown.

Mg_3Bi_2 is a promising system for flexible thermoelectric devices. It is a semimetal with topological surface states,^{16–18} a layered Zintl compound with a trigonal anti- α - La_2O_3 type structure (space group P-3m1).¹⁹ The low price and high elemental abundance, combined

with good thermoelectric properties close to room temperature, make it promising for wearable thermoelectrics.²⁰ Bulk single crystal Mg_3Bi_2 has been reported to exhibit high malleability, which is surprising since Mg-rich compounds are usually brittle, as well as good thermoelectric figure of merit compared to both organic and Bi_2Te_3 -based flexible devices operating near room temperature.^{19,21} Furthermore, polycrystalline Mg_3Bi_2 films have also been reported to be flexible.²⁰ Although there are many studies on the thermoelectric properties of Mg_3Bi_2 -based thin films, most neither report nor discuss stress,^{20,22–29} leaving important questions unanswered.

In this work, we investigate the effect of stress on the transport properties of Mg_3Bi_2 thin films, devising a strategy to vary stress states over a wide range. With various growth temperatures and using substrates with different thermal expansion coefficients compared to Mg_3Bi_2 , diverse stress states in the films are obtained. Elemental composition, crystal structure, and transport properties are investigated and discussed with respect to the estimated stress.

Mg_3Bi_2 thin films were deposited using direct current (dc) magnetron sputtering in a vacuum chamber (base pressure $< 2 \times 10^{-6}$ Pa). A detailed description of the deposition system is available elsewhere.³⁰ The power density was fixed at 0.57 W cm^{-2} for Bi (99.99%, MaTeck) and varied between 2.46 and 3.78 W cm^{-2} for Mg (99.95%, MaTeck) targets with a diameter of 50.8 mm . The Ar gas flow rate was kept constant at 80 sccm , corresponding to a working pressure of 0.5 Pa (3.5 mTorr). The substrate holder was maintained at temperatures between ambient temperature (no intentional heating) and 190°C , rotated at 15 rpm , and kept electrically floating. Some substrates were not used above 100°C growth temperature due to their lower thermal stability. The deposition time was 15 min , corresponding to a thickness of approximately 720 nm . The temperature was linearly interpolated from a calibration curve done at and above 200°C to the ambient temperature. To avoid discrepancies and variations between the substrates, the films were deposited simultaneously on all different substrates at each growth temperature and considered to have the same thickness and composition.

The substrates ($10 \times 10 \times 0.5 \text{ mm}^3$), thermoplastic and ceramic (crystalline), were selected to have a wide range of thermal expansion coefficients (Table I). The electrical resistivity ρ was measured at room temperature in a home-made van der Pauw setup with a Keithley 2400 source unit and a Keithley 2001 digital multimeter. The Seebeck coefficient S at room temperature was measured with a two-point probe method. The power factor S^2/ρ was calculated from these values. A more detailed method section is available in the [supplementary material](#).

TABLE I. The thermal expansion coefficients of the substrates and Mg_3Bi_2 .

Material	Linear thermal expansion coefficient (10^{-6} K^{-1})
Polycrystalline Al_2O_3 ³¹	7
$\text{MgO}(001)$ ³²	10
Mg_3Bi_2 ³³	22
Kapton ³⁴	34
Polyetherimide (PEI) ³⁵	56
Polyetheretherketone (PEEK) ³⁶	78

TABLE II. The growth temperature and the corresponding elemental composition and thickness of the studied thin films, as measured on Si (reference system). The elemental content is averaged from three separate areas on each sample, with a standard deviation given as an error.

Deposition temperature ($^\circ\text{C}$)	Mg (at. %)	Bi (at. %)	Thickness (nm)
Ambient	60.7 ± 0.2	39.3 ± 0.2	720
70	61.0 ± 0.7	39.0 ± 0.7	680
100	63.4 ± 0.1	36.6 ± 0.1	750
170	63.3 ± 0.4	36.7 ± 0.4	750
190	61.8 ± 0.2	38.2 ± 0.2	750

Table II contains the elemental composition and thickness of thin films grown on Si at various temperatures, as determined with EDS and SEM, respectively. Mg_3Bi_2 -based samples are often characterized by excess Mg, yielding an *n*-type semiconductor.³⁷ This is partially done intentionally to increase long-term stability since Mg loss occurs due to prolonged air exposure even at room temperature.³⁸ A slight excess of Mg has been shown to have a small effect on the thermoelectric properties of bulk samples.³⁹ The synthesis of thin films with the ideal composition is further complicated by the loss of Mg at higher growth temperatures due to its high vapor pressure, which has to be compensated by increasing the power for the Mg magnetron. Due to the sensitivity of this process, the elemental composition fluctuated slightly, as can be seen in Table II. Nevertheless, all samples are nearly stoichiometric (especially those below 100°C), being close to the ideal composition of 60 at. % Mg and 40 at. % Bi. Furthermore, no impurities were detected. The thin films with higher Mg content became slightly thicker as a result (Table II). The thickness of the thin film grown at 70°C is lower than expected, which could signify some variations in the uniformity of the thickness of each specimen, or simply a slight misalignment of the sample during the measurement of the cross section.

The set of XRD peaks from the film is the same regardless of the substrate, corresponding to the trigonal crystal structure of Mg_3Bi_2 , with the clearly distinct 00l, 010, 101, and 012 planes, with a similar shape and intensity. The presence of the 00l peaks becomes more pronounced starting at 100°C , implying that the films are increasingly textured. We have obtained a good phase purity for Mg_3Bi_2 on ceramic substrates and PEI at 100°C , and on all substrates above that growth temperature. This can be observed by the absence of XRD peaks attributed to pure bismuth (shaded peaks on Figs. 1 and 2), which are sharp and intense below 100°C on all substrates. At 100°C , these XRD peaks are greatly diminished for films deposited on PEEK and Kapton [Figs. 1(a) and 1(c)], and absent on films deposited on the other substrates [Figs. 1(b) and 2]. This could be explained by partial phase segregation at lower temperatures. A previous study has reported Mg_3Bi_2 thin films (bilayer Mg–Bi) to exhibit a sharp Bi-attributed peak when annealed at 150°C for 1 h.²⁴ Further annealing above the melting point of Bi yielded almost phase-pure samples. This is consistent with our results since the reported composition in the previous work was 64.7 at. % Mg and 35.3 at. % Bi.²⁴ We have detected a higher Mg content in samples with the pure Mg_3Bi_2 phase. Since the phase-pure Mg_3Bi_2 films are expected²⁰ to have more favorable transport

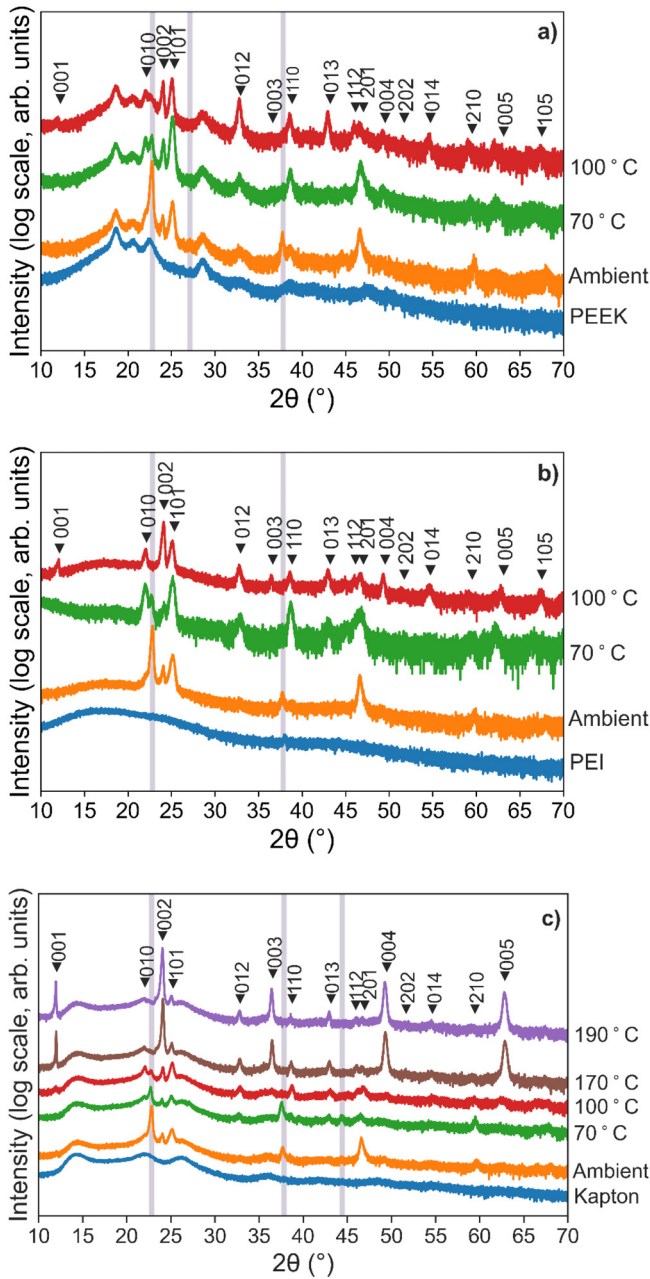


FIG. 1. X-ray diffraction patterns of Mg_3Bi_2 thin films deposited on thermoplastic substrates: (a) PEEK, (b) PEI, and (c) Kapton at different growth temperatures, with the pattern of each substrate at the bottom of each panel. The shaded lines indicate the positions of pure Bi peaks.

properties, even at the same stress state, we have highlighted these samples in a different color when discussing thermoelectric properties.

Figure 3 displays the SEM images of the surface morphology of films grown on Si(001) between ambient temperature and 190 °C. The changes due to temperature can be observed as the morphology changes from highly granular [Fig. 3(a)] at ambient temperature to

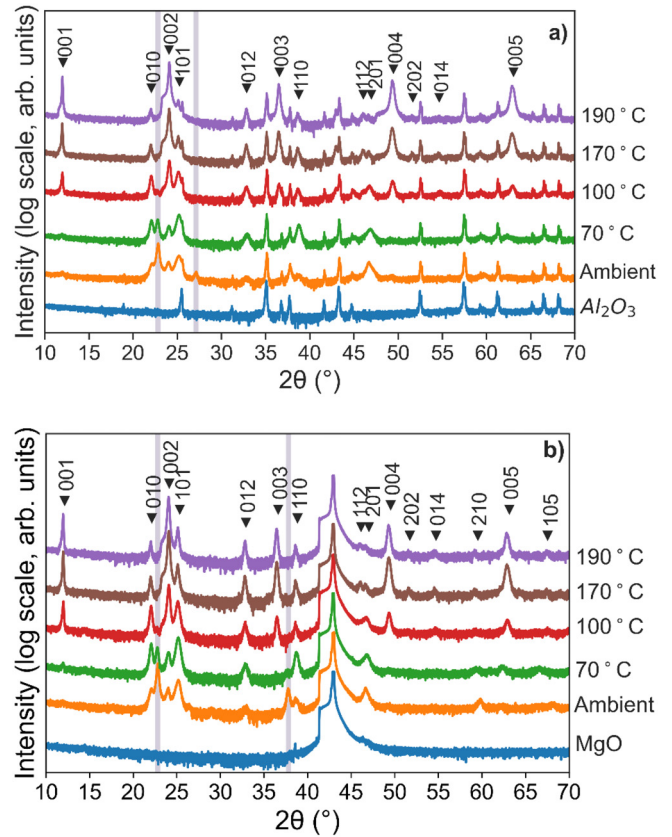


FIG. 2. X-ray diffraction patterns of Mg_3Bi_2 thin films deposited on ceramic substrates: (a) MgO(111) and (b) polycrystalline Al_2O_3 at different growth temperatures, with the pattern of each substrate at the bottom of each panel. The shaded lines indicate the positions of pure Bi peaks.

progressively more faceted with increasing temperature, starting at 70 °C [Fig. 3(b)]. At 100 °C, particle-like features appear on the surface of the thin films [Fig. 3(c)] only to become sparse and disappear at even higher temperatures [Fig. 3(d)]. Furthermore, the film grown on Si at 190 °C appears to buckle, as it can be seen from the cross section SEM image [Fig. 3(e)]. This is an indication of stress. The fact that the films can withstand thermal stresses without fracturing is an indication of the flexibility of the films.

As stated earlier, residual (total) stress in thin films consists of two components: thermal stress, caused by differences in thermal expansion between the film and substrate, and intrinsic stress, related to the growth process. The thermal component can be estimated using the difference in thermal expansion coefficients,

$$\sigma_{thermal} = E_f (\alpha_f - \alpha_s) \Delta T, \quad (1)$$

where E_f is the elastic modulus of the film, α_f and α_s are linear thermal expansion coefficients of the film and the substrate, respectively, and ΔT is the difference between the growth temperature and ambient temperature.¹⁵ On the other hand, the residual stress is challenging to quantify accurately. This is because key assumptions of the Stoney equation (curvature analysis) are not met in this work,^{15,40} including

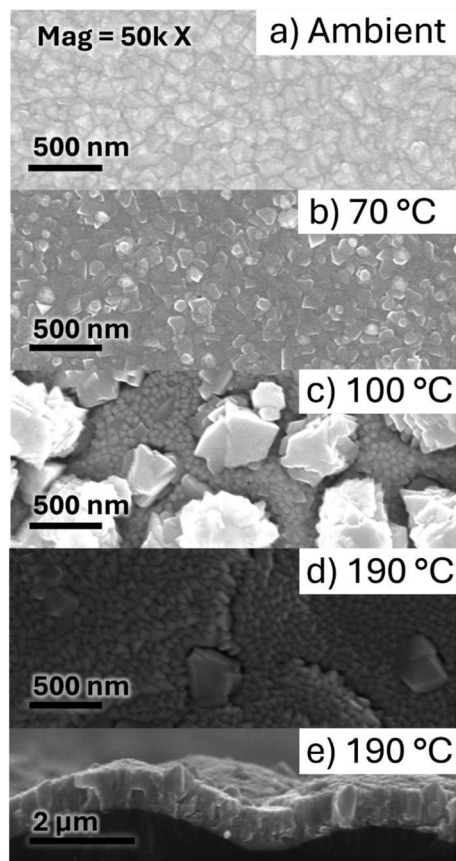


FIG. 3. Surface SEM images of films grown on Si(001) at (a) ambient (no intentional heating), (b) 70 °C, (c) 100 °C, (d) 190 °C, and (e) cross section image of the film grown on Si(001) at 190 °C.

that there is no measurement of the substrate's initial curvature (especially problematic for flexible polymeric substrates due to mounting and handling issues), and the fact that film deformations are neither infinitesimal nor purely spherical, and stress is not uniform throughout the film (for profilometric data, see Figs. S1–S4 in the [supplementary material](#)). Due to these limitations, the residual stress values are only approximate. Therefore, stress dependence on the transport properties is introduced as a temperature dependence, which primarily reflects the thermal stress component and serves as an indicator of stress evolution in thin films. This is further supported by the fact that the structural evolution is similar for various substrates (see [Figs. 1 and 2](#)). As the growth temperature increases, the thermal stress component increases according to Eq. (1), but due to relaxation effects (defects, buckling, and crack formation), the residual stress should decrease at some point. Hence, based on the SEM data (morphological changes in [Fig. 3](#)), phase purity (presence of Bi), and composition ([Table I](#)), 100 °C is taken as an inflection point.

[Figure 4](#) shows how the thermoelectric properties of films grown on crystalline (left panel) and thermoplastic (right panel) substrates are affected by thermal stress expressed through growth temperature. The samples with pure Mg_3Bi_2 phase are highlighted in orange, while the samples with Bi excess are marked with a yellow region instead,

which aligns with the inflection point at 100 °C, as argued earlier. For the samples grown on ceramic substrates, the power factor increases up to 100 °C, followed by a sharp decline [[Fig. 4\(a\)](#)]. This is mirrored by the behavior of the Seebeck coefficient [[Fig. 4\(c\)](#)]. A similar, if less pronounced trend, emerges for the power factor of the thin films on PEI and PEEK [[Fig. 4\(d\)](#)]. The Seebeck coefficients behave similarly to the samples grown on crystalline substrates, with two exceptions. First, the transport properties of the samples grown on Kapton peak already at ambient temperature and then decrease thereafter in an almost linear fashion. Second, the large compressive thermal stresses resulted in the Seebeck coefficient changing from p -type into n -type, as highlighted in blue in [Fig. 4\(e\)](#). Resistivity decreases until thermal stress corresponding to 70 °C, then it slowly increases. The samples grown on ceramic substrates exhibit lower resistivity [[Figs. 4\(c\) and 4\(f\)](#)].

The mean biaxial stress in the film, caused by cooling from the elevated growth temperature to ambient temperature, was modeled using the finite element method, see [Fig. 5](#). The modeled stress is consistent with the stress obtained using Eq. (1). [Figure S5](#) in the [supplementary material](#) shows the transport properties plotted as a function of thermal stress. Due to the aforementioned differences in the thermal expansion coefficients between the substrates (larger variation for thermoplastic substrates), the estimated thermal stress should vary between samples grown at the same growth temperature. The choice of substrate affects the properties of the film even when the thermal stress is virtually non-existent (the non-intentional heating is expected to be negligible, and the temperature gradient during Seebeck measurement was kept below 3 °C), as can be observed from samples synthesized at the ambient temperature ([Fig. S6](#)). This is expected, as the crystal structure and surface morphology of the sputtered films can be strongly affected by the substrate.⁴¹ For completeness, we also show the correlation between the average measured stress and the estimated thermal stress ([Fig. S7](#)), and the corresponding transport properties in [Fig. S8](#).

Stress can affect the Fermi level and therefore the Seebeck coefficient of a material.^{8–10} The value of the Seebeck coefficient depends on the energy difference between the Fermi level and the band edge—in semiconductors, it can be understood as a measure of the Fermi level.^{42,43} The persistent p -type nature of some stoichiometric Zintl phases has been attributed to an intrinsic defect pinning the Fermi level inside the valence band and preventing its shift into the conduction band.^{44,45} According to the literature, the stoichiometric Mg_3Bi_2 is a p -type semiconductor, while a small excess of Mg is enough to turn it into n -type.⁴⁶ In our earlier work, we have observed the persistent p -type nature of Mg_3Bi_2 with larger Mg excess, implying that the actual composition required for the transition into n -type seems to be heavily dependent on the synthesis process.⁴⁷ Here, we observed that three samples with large compressive stress changed their nature from p -type into n -type, as can be seen in [Fig. 4\(e\)](#). Other samples with essentially identical compositions remained p -type. This highlights the importance of reporting stress when investigating transport properties of a material.^{48,49}

There is a wide variation in the power factor values of thin films with similar crystal structure due to stress. Since the structure of the films is similar, the other factor to consider is the composition. There is a study showing that changing the Bi content from the stoichiometric composition by 2% can significantly decrease the power factor of n -type Mg_3Bi_2 thin films.²⁰ This implies that the changes due to stress

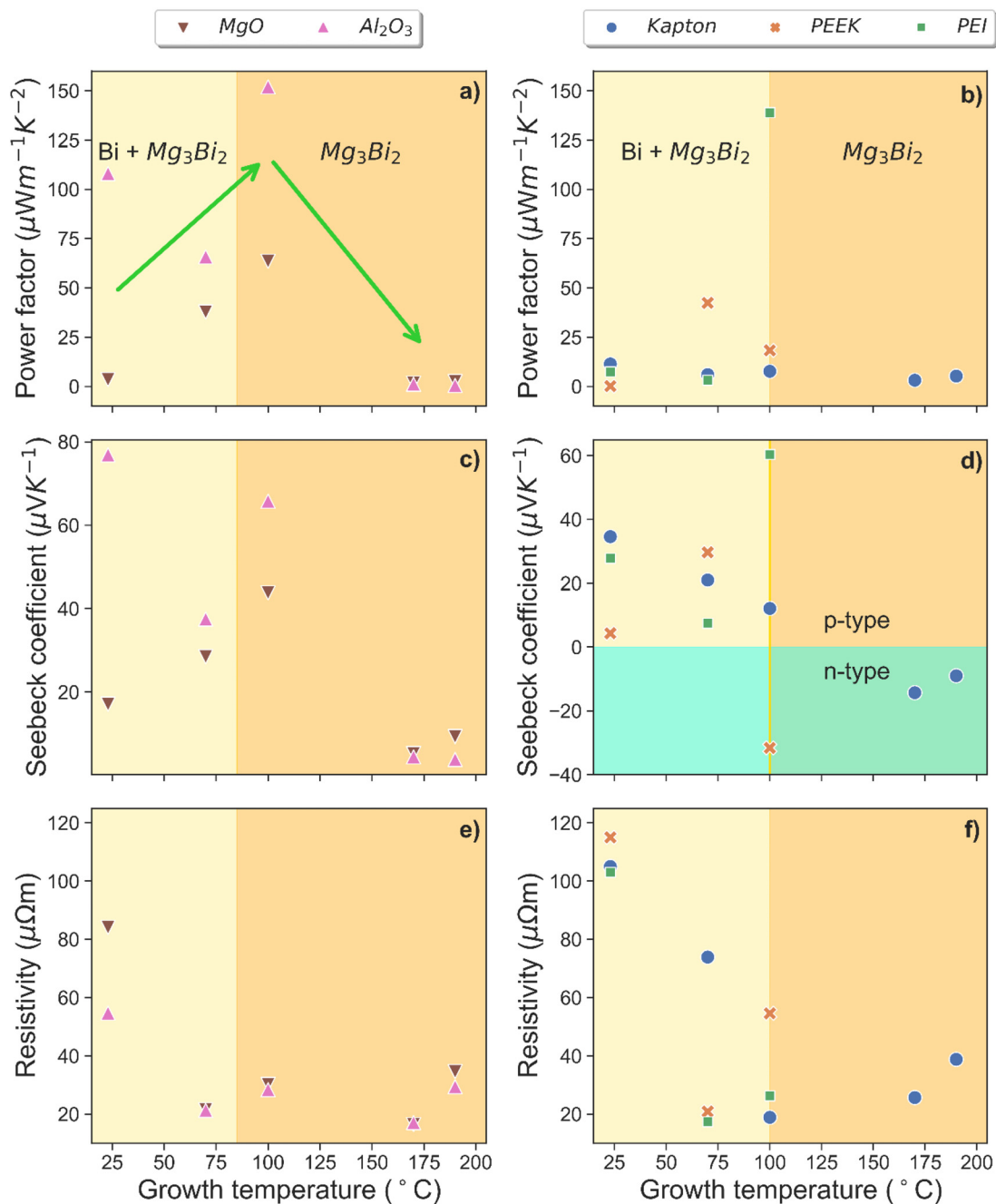


FIG. 4. The thermolectric properties as a function of stress expressed as growth temperature for Mg_3Bi_2 thin films: (a) and (b) power factor, (c) and (d) Seebeck coefficient, and (e) and (f) resistivity of the films deposited on crystalline (tensile thermal stress) and thermoplastic (compressive thermal stress) substrates, respectively. The arrows indicate the proposed trends.

might have been even more noticeable if the composition of the films was identical. Films grown on each substrate have a clear local maximum power factor, as indicated by the green arrows in Fig. 4(a), highlighting the trend for films grown on ceramic substrates. It is our assumption that at higher stresses, the relaxation mechanisms cause

deformation or even cracks to appear, leading to decrease in the Seebeck coefficient and therefore the power factor. That trend is harder to perceive for thermoplastic substrates [Fig. 4(d)] due to a larger variation in thermal expansion coefficients, which shifts the optimal stress to lower growth temperatures. The estimated tensile stresses resulting

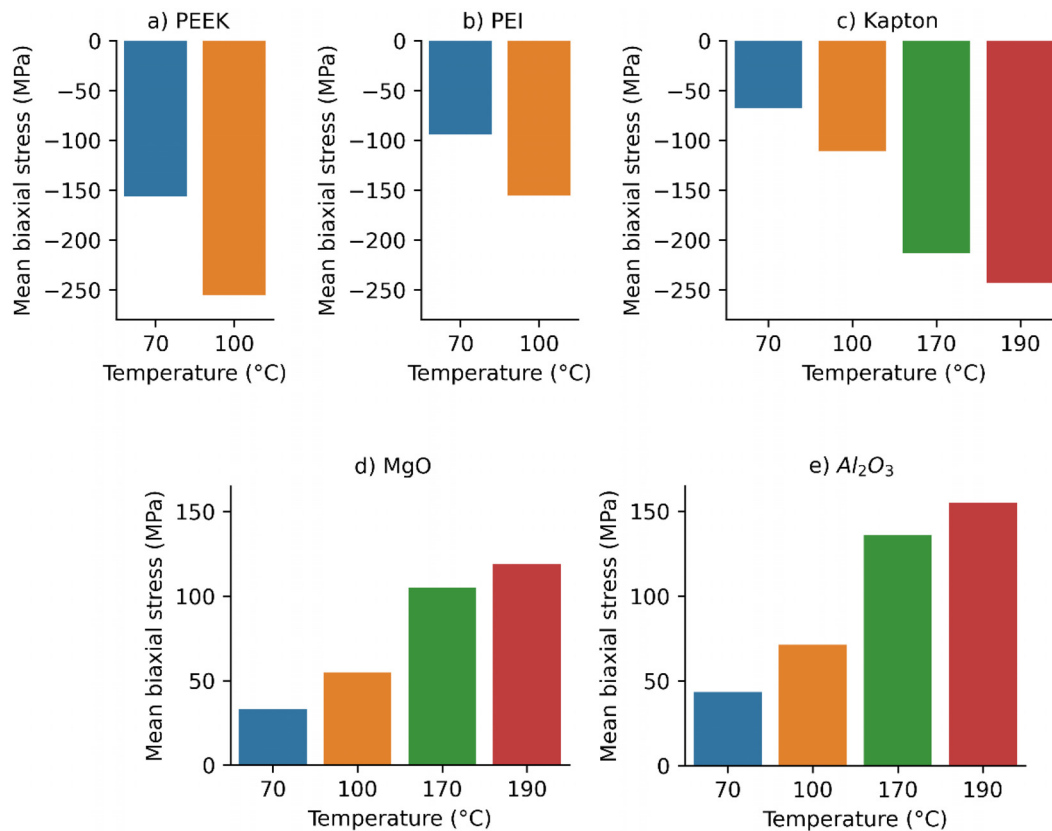


FIG. 5. The mean (in-plane) biaxial stress in the films as a function of growth temperature and substrate, simulated using finite elements.

in the optimal transport properties are close to twice the value of the corresponding compressive stresses. The negative effects of high stress can also be observed in Fig. 4, as the power factor falls below $6 \mu\text{W m}^{-1} \text{K}^{-2}$ at the highest stresses. The lowest power factor is 0.2, while the highest one is $152 \mu\text{W m}^{-1} \text{K}^{-2}$. The stress could help explain the wide scatter (between 80 and $200 \mu\text{W m}^{-1} \text{K}^{-2}$) of the reported^{20,22–28} power factor values at room temperature for Mg_3Bi_2 thin films.

In conclusion, we have investigated how the thermoelectric properties of Mg_3Bi_2 thin films are affected by stress. Through selecting different combinations of growth temperature and substrates with specific thermal expansion coefficients, we control the thermal stress. The power factor peaks for moderate stress values for samples on both crystalline and thermoplastic substrates, while excessive stress results in a steep decrease. We suggest that a relaxation mechanism occurs, introducing defects to reduce residual stress. Films with similar crystal structure exhibit power factors between 0.2 and $152 \mu\text{W m}^{-1} \text{K}^{-2}$ due to variations in stress. The variation of the power factor by four orders of magnitude can easily yield a large scatter in measured literature data as well as affect the performance of wearable devices.

See the [supplementary material](#) for a more detailed description of the methods used, the curvature measurements of the samples analyzed using the Stoney equation, as well as discussion on stress based on these measurements.

This work was financially supported by the Olle Engkvist Foundation (Project No. 217-0023). P.E. and A.F. acknowledge funding from the Swedish Government Strategic Research Area in Materials Science on Functional Materials at Linköping University (Faculty Grant SFO-Mat-LiU No. 2009 00971), the Knut and Alice Wallenberg foundation through the Wallenberg Academy Fellows program (No. KAW-2020.0196), and the Swedish Research Council (VR) under Project No. 2021-03826, and the Swedish Energy Agency under Project No. 52740-1.

AUTHOR DECLARATIONS

Conflict of Interest

The authors have no conflicts to disclose.

Author Contributions

Grzegorz Sadowski: Formal analysis (lead); Investigation (lead); Visualization (lead); Writing – original draft (lead); Writing – review & editing (equal). **Arnaud le Febvrier:** Formal analysis (supporting); Investigation (supporting); Methodology (supporting); Writing – review & editing (equal). **Johan Hektor:** Formal analysis (supporting); Supervision (equal); Writing – review & editing (equal). **Per Eklund:** Formal analysis (supporting); Investigation (supporting); Methodology (supporting); Writing – review & editing (equal).

Denis Music: Conceptualization (lead); Formal analysis (supporting); Funding acquisition (lead); Supervision (equal); Writing – review & editing (equal).

DATA AVAILABILITY

The data that support the findings of this study are available within the article and its [supplementary material](#).

REFERENCES

- ¹X. Li, K. Cai, M. Gao, Y. Du, and S. Shen, *Nano Energy* **89**, 106309 (2021).
- ²Y. Du, J. Xu, B. Paul, and P. Eklund, *Appl. Mater. Today* **12**, 366–388 (2018).
- ³Y. Wang, L. Yang, X.-L. Shi, X. Shi, L. Chen, M. S. Dargusch, J. Zou, and Z.-G. Chen, *Adv. Mater.* **31**, 1807916 (2019).
- ⁴S. Yang, P. Qiu, L. Chen, and X. Shi, *Small Sci.* **1**, 2100005 (2021).
- ⁵M. Stoppa and A. Chiolerio, *Sensors* **14**, 11957–11992 (2014).
- ⁶M. J. Mirshojaeian Hosseini and R. A. Nawrocki, *Micromachines* **12**, 655 (2021).
- ⁷E. S. Itskevich, L. M. Kashirskaya, and V. F. Kraidenov, *Semiconductors* **31**, 276–278 (1997).
- ⁸J. L. Hoyt, H. M. Nayfeh, S. Eguchi, I. Aberg, G. Xia, T. Drake, E. A. Fitzgerald, and D. A. Antoniadis, in *Technical Digest—International Electron Devices Meeting* (IEEE, 2002), pp. 23–26.
- ⁹J. Xie, S. Mita, A. Rice, J. Tweedie, L. Hussey, R. Collazo, and Z. Sitar, *Appl. Phys. Lett.* **98**, 202101 (2011).
- ¹⁰H. Li, L. Martinelli, F. Cadiz, A. Bendounan, S. Arscott, F. Sirotti, and A. C. H. Rowe, *Appl. Surf. Sci.* **478**, 284–289 (2019).
- ¹¹T. Thonhauser, T. J. Scheidmantel, J. O. Sofo, J. V. Badding, and G. D. Mahan, *Phys. Rev. B* **68**, 085201 (2003).
- ¹²D. A. Polvani, J. F. Meng, N. V. Chandra Shekar, J. Sharp, and J. V. Badding, *Chem. Mater.* **13**, 2068–2071 (2001).
- ¹³M. Lifshitz, *Sov. Phys. JETP* **11**, 1130–1135 (1960).
- ¹⁴E. Chason and P. R. Guduru, *J. Appl. Phys.* **119**, 191101 (2016).
- ¹⁵M. R. Ardigo, M. Ahmed, and A. Besnard, *Adv. Mater. Res.* **996**, 361–366 (2014).
- ¹⁶T. Zhou, M. Tong, Y. Zhang, X. Xie, Z.-Y. Wang, T. Jiang, X.-G. Zhu, and X.-C. Lai, *Phys. Rev. B* **103**, 125405 (2021).
- ¹⁷T. Zhou, M. Tong, X. Xie, Y. Yu, X. Zhu, Z.-Y. Wang, and T. Jiang, *J. Phys. Chem. Lett.* **11**, 6475–6481 (2020).
- ¹⁸T. Zhou, X.-G. Zhu, M. Tong, Y. Zhang, X.-B. Luo, X. Xie, W. Feng, Q. Chen, S. Tan, Z.-Y. Wang, T. Jiang, Y. Tang, X.-C. Lai, and X. Yang, *Chin. Phys. Lett.* **36**, 117303 (2019).
- ¹⁹M. Hu, J. Yang, Y. Wang, J. Xia, Q. Gan, S. Yang, J. Xu, S. Liu, W. Yin, B. Jia, L. Xie, H. Li, and J. He, *Nat. Commun.* **16**, 128 (2025).
- ²⁰B. Hu, X.-L. Shi, T. Cao, S. Liu, M. Zhang, W. Lyu, L. Yin, T. Tesfamichael, Q. Liu, and Z.-G. Chen, *Adv. Sci.* **11**, 2409788 (2024).
- ²¹P. Zhao, W. Xue, Y. Zhang, S. Zhi, X. Ma, J. Qiu, T. Zhang, S. Ye, H. Mu, J. Cheng, X. Wang, S. Hou, L. Zhao, G. Xie, F. Cao, X. Liu, J. Mao, Y. Fu, Y. Wang, and Q. Zhang, *Nature* **631**, 777–782 (2024).
- ²²S. Bano, Y. Peng, T. Aizawa, R. Chetty, and T. Mori, *J. Mater. Chem. C* **11**, 15130–15137 (2023).
- ²³G. Sadowski, Y. Zhu, R. Shu, T. Feng, A. le Febvrier, D. Music, W. Liu, and P. Eklund, *Appl. Phys. Lett.* **120**, 051901 (2022).
- ²⁴J. Tani and H. Ishikawa, *Mater. Lett.* **331**, 133460 (2023).
- ²⁵W. Fang, W. Zhu, Y. Shao, P. Zheng, and J. Si, *Appl. Surf. Sci.* **596**, 153602 (2022).
- ²⁶Y. Shao, P. Zheng, T. Dong, L. Wei, H. Wu, and J. Si, *Vacuum* **220**, 112791 (2024).
- ²⁷Y. Ran, W. Ma, H. Yu, W. Li, D. Zhou, F. Wang, N. Gao, Z. Yu, and K. Tai, *J. Alloys Compd.* **985**, 174028 (2024).
- ²⁸J. W. C. Reinders, C. Roldán-Carmona, H. J. Bolink, and F. Palazon, *ACS Appl. Energy Mater.* **6**, 10327–10332 (2023).
- ²⁹G. Sadowski, R. Shu, A. le Febvrier, Z. Han, D. Music, W. Liu, and P. Eklund, *J. Vac. Sci. Technol., A* **41**, 043409 (2023).
- ³⁰A. le Febvrier, L. Landäl, T. Liersch, D. Sandmark, P. Sandström, and P. Eklund, *Vacuum* **187**, 110137 (2021).
- ³¹AzoM, *Alumina—Aluminium Oxide—Al₂O₃—A Refractory Ceramic Oxide* (AZoM, 2001).
- ³²R. Reeber, K. Goessel, and K. Wang, *Eur. J. Mineral.* **7**, 1039–1048 (1995).
- ³³M. T. Agne, K. Imasato, S. Anand, K. Lee, S. K. Bux, A. Zevalkink, A. J. E. Rettie, D. Y. Chung, M. G. Kanatzidis, and G. J. Snyder, *Mater. Today Phys.* **6**, 83–88 (2018).
- ³⁴DuPont, *Kapton HN* (DuPont, 2024).
- ³⁵Goodfellow Cambridge Ltd, *Supplier Data: Polyetherimide (PEI)* (Goodfellow Cambridge Ltd, 2003).
- ³⁶Goodfellow Cambridge Ltd, *Supplier Data: Polyetheretherketone (PEEK)* (Goodfellow Cambridge Ltd, 2003).
- ³⁷S. Zhou, Y.-R. Yin, Y. Tian, X.-C. Liu, Q. Liu, B. Li, and S.-Q. Xia, *ACS Appl. Mater. Interfaces* **16**, 28886–28895 (2024).
- ³⁸J. Zhang, L. R. Jorgensen, L. Song, and B. B. Iversen, *ACS Appl. Mater. Interfaces* **14**, 31024–31034 (2022).
- ³⁹J. Shuai, B. Ge, J. Mao, S. Song, Y. Wang, and Z. Ren, *J. Am. Chem. Soc.* **140**, 1910–1915 (2018).
- ⁴⁰G. C. A. M. Janssen, M. M. Abdalla, F. van Keulen, B. R. Pujada, and B. van Venrooy, *Thin Solid Films* **517**, 1858–1867 (2009).
- ⁴¹H. Khachatryan, S.-N. Lee, K.-B. Kim, H.-K. Kim, and M. Kim, *J. Phys. Chem. Solids* **122**, 109–117 (2018).
- ⁴²G. J. Snyder, A. Pereyra, and R. Gurunathan, *Adv. Funct. Mater.* **32**, 2112772 (2022).
- ⁴³A. Zevalkink, D. M. Smiadak, J. L. Blackburn, A. J. Ferguson, M. L. Chabinyk, O. Delaire, J. Wang, K. Kovnir, J. Martin, L. T. Schelhas, T. D. Sparks, S. D. Kang, M. T. Dylla, G. J. Snyder, B. R. Ortiz, and E. S. Toberer, *Appl. Phys. Rev.* **5**, 021303 (2018).
- ⁴⁴S. Ohno, K. Imasato, S. Anand, H. Tamaki, S. D. Kang, P. Gorai, H. K. Sato, E. S. Toberer, T. Kanno, and G. J. Snyder, *Joule* **2**, 141–154 (2018).
- ⁴⁵H. Tamaki, H. K. Sato, and T. Kanno, *Adv. Mater.* **28**, 10182–10187 (2016).
- ⁴⁶J. Mao, H. Zhu, Z. Ding, Z. Liu, G. A. Gamage, G. Chen, and Z. Ren, *Science* **365**, 495–498 (2019).
- ⁴⁷K. Imasato, M. Wood, S. Anand, J. J. Kuo, and G. J. Snyder, *Adv. Energy Sustainable Res.* **3**, 2100208 (2022).
- ⁴⁸F. Salleh, Y. Suzuki, K. Miwa, and H. Ikeda, in *International Conference on QiR* (IEEE, 2013), pp. 47–50.
- ⁴⁹M. Markwitz, P. P. Murmu, S. Y. Back, T. Mori, J. V. Kennedy, and B. J. Ruck, *Mater. Today Phys.* **46**, 101513 (2024).